Contrib Mineral Petrol (1994) 117:229–240

E. Dachs

Annite stability revised. 1. Hydrogen-sensor data for the reaction annite = sanidine + magnetite + H_2

Received: 27 July 1993 / Accepted: 16 February 1994

Abstract In P-T-logf_{O_2} space, the stability of annite (ideally $KFe_3^{2+}(OH)_2AlSi_3O_{10}$) at high f_{O_2} (low f_{H_2}) is limited by the reaction:

annite = sanidine + magnetite + H_2. (1)

Using the hydrogen-sensor technique, the equilibrium f_{H_2} of this reaction was measured between 500 and 800° C at 2.8 kbar in 50° C intervals. Microbrobe analyses of the reacted annite + sanidine + magnetite mixtures show that tetrahedral positions of annite have a lower Si/Al ratio than the ideal value of 3/1. Silicon decreases from ~2.9 per formula unit at low temperatures to ~2.76 at high temperatures. As determined by Mössbauer spectroscopy in three experimental runs, the Fe^{3+} content of annite in the equilibrium assemblage is 11% ± 3. A least squares fit to the hydrogen-sensor data gives $\Delta H_R^0 = 50.269 \pm 3.987$ kJ and $\Delta S_R^0 = 83.01 \pm 4.35$ J/K for equilibrium (1). The hydrogen-sensor data are consistent with temperature half brackets determined in the classical way along the nickel-nickel oxide (NNO) and quartz-fayalite-magnetite (QFM) buffers with a mixture of annite + sanidine + magnetite for control. Compared to published oxygen buffer reversals, agreement is only found at high temperature and possible reasons for that discrepancy are discussed. The resulting slope of equilibrium (1) in log$f_{O_2} - T$ dimensions is considerably steeper than previously determined and between 400 and 800° C only intersects with the QFM buffer curve. Based on the hydrogen-sensor data and on the thermodynamic dataset of Berman (1988, and TWEEQ data base) for sanidine, magnetite and H_2, the deduced standard-state properties of annite are: $H_f^0 = -5127.376 \pm 5.279$ kJ and $S^0 = 422.84 \pm 5.29$ J/(mol K). From the recently published unit cell refinements of annites and their Fe^{3+} contents, determined by Mössbauer spectroscopy (Redhammer et al. 1993), the molar volume of pure annite was constrained as 15.568 ± 0.030 J/bar. A revised stability field for annite is presented, calculated between 400 and 800° C.

Edgar Dachs
Institut für Mineralogie, Universität Salzburg,
Hellbrunnerstrasse 34, A-5020 Salzburg, Austria

Editorial responsibility: W. Schreyer

Introduction

Equilibria involving biotite play an important role in many aspects of metamorphic and magmatic petrology. In most biotites the iron-endmember annite, $KFe_3(OH)_2AlSi_3O_{10}$, is a major component and its thermodynamic standard-state properties are necessary input quantities in many applications, like geothermobarometry. Our knowledge concerning phase relations and stability of annite goes back to the pioneering experimental work of Eugster and Wones (1962), who studied properties and phase relations of annite in the subsolidus range, employing the solid-oxygen buffer technique, introduced by Eugster (1957, 1959), to control annite redox reactions at high pressure and temperature. A major part of their experiments was done on the upper log$f_{O_2} - T$ stability limit of annite, given by the reaction:

annite = sanidine + magnetite + H_2, (1)

for which temperature brackets along the HM (hematite-magnetite), NNO (nickel-nickel oxide), QFM (quartz-fayalite-magnetite) and MW (magnetite-wuestite) oxygen buffers were determined. Further equilibrium data came from Rutherford (1969), providing another temperature brackets at the QFM- and G-CH (graphite-methane) buffers and from Hewitt and Wones (1981), at HM (and at 50 bars P_{H_2}). Hewitt and

Wones (1984) performed a revision of equilibrium (1) correcting it for the Fe^{3+} content of annite, as measured by Partin et al. (1983) in synthetic annites annealed at various f_{H_2}-conditions.

Experiments with annite are generally complicated by the fact that the pure ideal endmember does not exist. "Pure" annite always contains some Fe^{3+}. As pointed out by Hazen and Wones (1972), octahedral cations in trioctahedral natural micas are not observed to exceed a mean cationic radius of 0.76 Å. Because pure annite with only Fe^{2+} would have an average octahedral ionic radius greater than this critical value, they predicted that even the most reduced annite should contain >12% octahedral (oc) Fe^{3+} in order to lower the mean octahedral ionic radius below this limit. Using Mössbauer spectroscopy their hypothesis was verified by Wones et al. (1971) and later in annealing experiments of Ferrow and Annersten (1984), and the recent study of Redhammer et al. (1993), showing a minimum Fe^{3+} content around 11% in synthetic annite even at the most reducing conditions, increasing linearly with f_{O_2}. The oxyannite substitution ($Fe^{2+} + OH^- = Fe^{3+} + O^{2-}$, Eugster and Wones 1962), and a vacancy substitution ($3Fe^{2+}_{oc} = 2Fe^{3+}_{oc} + \text{vacancy}_{oc}$), are regarded as the most probable mechanisms responsible for the incorporation of octahedral Fe^{3+} into annite. In the absence of reliable data on OH contents of natural and synthetic Fe-biotites, the oxyannite substitution is generally assumed to be the more important one. However, Redhammer et al. (1993) present evidence based on infra-red (IR) spectroscopy, demonstrating that increasing Fe^{3+} correlates with increasing octahedral vacancies. Both vacancies and Fe^{3+} show a preference for the M1 position. A Ferri-Tschermak's substitution ($Fe^{2+}_{oc} + Si^{4+}_{tet} = Al^{3+}_{tet} + Fe^{3+}_{oc}$) may be another mechanism in a system with excess Al, where the annite composition can shift off its ideal tetrahedral (tet) Si/Al = 3/1 ratio.

The available experimental data of annite redox equilibria have not been incorporated into the data bases of internally consistent standard-state properties of minerals up to now (e.g. Bermann 1988, 1990; Holland and Powell 1990), mainly because an appropriate activity model for H_2O-H_2 fluids was not at hand. This gap was filled recently by Grevel and Chatterjee (1992), which is a prerequisite to convert $\log f_{O_2}$-data into corresponding $\log f_{H_2}$ and vice versa. Instead, the annite data were retrieved from Fe-Mg exchange experiments between biotite and another Fe-Mg silicate (garnet, orthopyroxene and chlorite, Ferry and Spear 1978; Fonarev and Konilov 1986; Powell 1985), which has the considerable disadvantage that they are dependent on the activity model adopted for this second Fe-Mg phase as well as on assumptions concerning Fe-Mg mixing in biotite itself.

In the course of the experimental work done by Redhammer et al. (1993) it turned out that some experiments were not in agreement with the upper $\log f_{O_2}$–T stability limit of annite as given by Eugster and Wones (1962). This was the motivation to reinvestigate this boundary, which was done utilizing the hydrogen-sensor technique in most experiments (Chou 1987a) and subordinate the classical oxygen buffers too. Equilibrium data were gathered from 500 to 800° C in 50° C steps. Run products are characterized by microprobe analyses, unit cell parameters and Fe^{3+} contents. Results obtained for reaction (1) are reported in this paper and are used to extract annite standard-state properties.

Experimental methods

Hydrothermal apparatus

Conventional cold-seal pressure vessels, 23.5 cm long × 4 cm (OD) × 0.7 cm (ID), fabricated from RENE-41 alloy were used in all experiments. Filler rods of Ni were placed inside the vessel to reduce the volume of the pressure medium (which was water, mixed with a highly dispersed oil in the proportion 20:1). Routine pressure measurements (accurate to approximately ±50 bars) were performed daily with an electrical resistance gauge, which was calibrated periodically against a Heise manometer. Sheathed Ni/Ni-Cr thermocouples, inserted in a small well at the base of the vessel orientated parallel to the central bore, were used to measure temperature. The temperature gradient along the first 4 cm of the vessel bore and the temperature difference to the external thermocouple were calibrated for each furnace at 500, 625 and 750° C at 2 and 5 kbar with an assembly consisting of three internal thermocouples, whose ends were spaced in 2 cm intervals along a 4 cm long gold tube, starting at the bottom of the vessel. Depending on the furnaces (horizontal Kanthal-wired tube-furnaces), temperature differences were observed to increase with temperature and in the worst case amounted to 4 and 8° C at low and high temperatures, respectively, but were mostly better (typically 3 and 5° C). Each thermocouple was calibrated against a standard thermocouple, and was found to deviate by a maximum of 4° C. From these observations the final temperature during a run at the external thermocouple was choosen in such a way that it corresponded to the desired value in the middle of the gold tube. Temperatures given in Table 1 are estimated accurate to ±5° C. Temperature control was achieved by connecting each thermocouple to an electric controler (Phillips KS-4580), equipped with a serial interface allowing communication with a computer. This PC was used as on-line control unit of run temperatures and as an easily handled tool to start and turn off experiments. The vessels were cooled down to temperatures <100° C under a stream of compressed air within ca. 5 min.

Starting materials

Presynthesized annite and sanidine and reagent-grade magnetite (Johnson and Matthey) were used as starting materials. Starting compositions for annite and sanidine were prepared by the gel method of Hamilton and Henderson (1968), using nitrates as the source for Al and Fe ($Al(NO_3)_3 \cdot 9H_2O$ and $Fe(NO_3)_3 \cdot 9H_2O$, checked before by titration), K_2CO_3 for K and $C_8H_{20}O_4Si$ for Si. Before synthesis the annite gel was reduced under a H_2 stream at 600° C to convert iron to the divalent state.

Annites were synthesized at 600° C/5 or 4 kbar for 2–3 weeks at redox conditions of the bomb (these were relatively new, and produced $\log f_{O_2} \sim -20.8$, as measured by hydrogen sensors, described later). As checked by optical microscopy, X-ray diffraction (XRD)

Table 1 Hydrogen-sensor data for the equilibrium annite = sanidine + magnetite + H_2 at 2.8 kbar. Runs with sensor A are labelled *A* at the end, those with sensor B *B*, reference experiments with the NNO buffer according *RA* and *RB*. Experiments have been repeated once for 600 and 700° C and twice for 750° C (*A* + *S* + *M* mixture of annite + sanidine + magnetite, *n* number of Cl^- measurements per sensor). (M_{Cl^-}): molarity of Cl^- measured by chloridometer after quench, the mean value is given in the column ($M^m_{Cl^-}$, lnK* is a modified equilibrium constant, combining $\ln f_{H_2}$ with all thermodynamic terms except ΔH^0_R and ΔS^0_R. For further explanations see text

Run number	*T* [° C]	duration [h]	preparate	start solution	*n*	(M_{Cl^-}) 1	2	3	4	($M^m_{Cl^-}$) (1σ)	$(f_{H_2})^{P,T}$ (1σ)	$\mathrm{Log}(f_{O_2})^{P,T}$ (1σ)	lnK* (1σ)
EQ1C14-A	500	196	A + S + M	aqu. dest.	3	0.576	0.586	0.586		0.5843	11.569[b]	−23.830	2.350
EQ1CB-B	500	196	A + S + M	1 M HCl	3	0.580	0.586	0.592		(0.0056)	(0.832)	(0.063)	(0.100)
EQ1C14-RA	500	196	Ni + NiO	aqu. dest	3	0.316	0.328	0.326		0.3167	3.054	−22.673[a]	
Eq1Cl4-RB	500	196	Ni + NiO	1 M HCl	3	0.308	0.310	0.312		(0.0085)	(0.067)	(0.019)	
EQ1C17-A	50	165	A + S + M	aqu.dest.	3	0.634	0.634	0.640		0.6451	14.667	−21.829	2.473
EQ1C17-B	550	165	A + S + M	1 M HCl	4	0.640	0.656	0.652	0.660	(0.0107)	(1.162)	(0.069)	(0.129)
EQ1C17-RA	550	165	Ni + NiO	aqu. dest	4	0.342	0.346	0.354	0.358	0.3548	4.201	−20.743	
EQ1C17-RB	550	165	Ni + NiO	1 M HCl	4	0.348	0.352	0.362	0.376	(0.0107)	(0.094)	(0.018)	
EQ1C11-A1	600	69	A + S + M	aqu. dest.	3	0.746	0.754	0.734		0.7483	19.431	−20.129	3.041
EQ1C11-B1	600	69	A + S + M	1 M HCl	3	0.754	0.752	0.750		(0.0076)	(1.213)	(0.055)	(0.096)
EQ1C11-A2	600	72	A + S + M	aqu. dest.	4	0.692	0.706	0.702	0.710	0.7058	17.225	−20.025	2.920
EQ1C11-B2	600	72	A + S + M	1 M HCl	4	0.692	0.710	0.710	0.724	(0.0106)	(1.148)	(0.058)	(0.099)
EQ1C11-RA	600	68	Ni + NiO	aqu. dest.	4	0.410	0.392	0.422	0.416	0.4055	5.517	−19.035	
EQ1C11-RB	600	68	Ni + NiO	1 M HCl	4	0.404	0.398	0.394	0.408	(0.0106)	(0.108)	(0.017)	
EQ1C16-A	650	72	A + S + M	auq. dest.	4	0.924	0.956	0.948	0.974	0.9688	24.985	−18.623	3.238
EQ1C16-B	650	72	A + S + M	2 M HCl	4	0.982	0.974	0.994	0.998	(0.0248)	(1.792)	(0.063)	(0.128)
EQ1C16-RA	650	72	Ni + NiO	aqu. dest	4	0.500	0.514	0.524	0.528	0.5190	6.982	−17.514	
EQ1C16-RB	650	72	Ni + NiO	1 M HCl	4	0.512	0.516	0.530	0.528	(0.0104)	(0.128)	(0.016)	
EQ1C12-A1	700	56	A + S + M	aqu. dest.	3	1.622	1.620	1.608		1.6010	64.287	−17.905	3.990
EQ1C12-B1	700	56	A + S + M	2 M HCl	3	1.556	1.580	1.620		(0.0271)	(4.505)	(0.062)	(0.096)
EQ1C12-A2	700	66	A + S + M	aqu. dest.	3	1.400	1.418	1.412		1.3833	47.542	−17.642	3.688
EQ1C12-B2	700	66	A + S + M	2 M HCl	3	1.338	1.360	1.372		(0.0317)	(3.694)	(0.068)	(0.102)
EQ1C12-RA	700	56	Ni + NiO	aqu. dest.	4	0.606	0.600	0.580	0.608	0.5983	8.573	−16.151	
EQ1C12-RB	700	56	Ni + NiO	1 M HCl	4	0.574	0.594	0.624	0.600	(0.0159)	(0.148)	(0.015)	
EQ1C15-A1	750	24	A + S + M	aqu. dest.	3	1.686	1.706	1.740		1.7200	54.255	−16.371	3.874
EQ1C15-B1	750	24	A + S + M	4 M HCl	3	1.716	1.728	1.744		(0.0219)	(4.503)	(0.073)	(0.114)
EQ1C15-A2	750	25	A + S + M	aqu. dest.	4	1.842	1.866	1.896	1.888	1.9130	67.659	−16.564	4.095
EQ1C15-B2	750	25	A + S + M	4 M HCl	4	1.932	1.948	1.960	1.972	(0.0470)	(6.633)	(0.086)	(0.126)
EQ1C15-A3	750	41	A + S + M	aqu. dest.	4	2.128	2.148	2.174	2.285	2.1167	83.541	−16.749	4.306
EQ1C15-B3	750	41	A + S + M	4 M HCl	4	1.986	2.042	2.040	2.130	(0.0937)	(11.427)	(0.121)	(0.158)
EQ1C15-RA	750	24	Ni + NiO	aqu. dest.	3	0.732	0.740	0.742		0.764	10.280	−14.922	
EQ1C15-RB	750	24	Ni + NiO	2 M HCl	4	0.760	0.780	0.798	0.796	(0.0275)	(0.165)	(0.014)	
EQ1C13-A	800	20	A + S + M	2 M HCl	2	2.545	2.396			2.4748	103.565	−15.686	4.473
EQ1C13-B	800	20	A + S + M	4 M HCl	2	2.428	2.530			(0.0739)	(9.852)	(0.084)	(0.122)
EQ1C13-RA	800	20	Ni + NiO	aqu. dest.	3	0.840	0.862	0.874		0.8723	12.062	−13.809	
EQ1C13-RB	800	20	Ni + NiO	2 M HCl	3	0.878	0.884	0.896		(0.0194)	(0.180)	(0.013)	

[a] $\mathrm{Log}(f_{O_2})^{P,T}$ for the Ni/NiO reference experiments is based on emf measurements of O'Neill (1987a) corrected to the experimental pressure of 2.8 kbar

[b] Calculated according to Eq. (3)

and microprobe, fine grained annite (< 5 μm) formed without significant amounts of other phases (in some runs $< \sim 5$ vol.% fayalite was found). Detailed information concerning chemical composition, unit cell and Mössbauer parameters of annites synthesized at different $\log f_{O_2}$–T conditions recently have been given by Redhammer et al. (1993).

Synthesis conditions for sanidine were 700° C/2 kbar/1–2 weeks. A unit cell refinement of one product, which was usually relatively coarse grained, gave $a_0 = 8.6108$ (8) Å, $b_0 = 13.0254$ (11) Å, $c_0 = 7.1841$ (6) Å, and $\beta = 115.981$ (7)°, demonstrating that completely disordered high sanidine has formed.

All experiments started with ~ stoichiometric mixtures of annite + sanidine + magnetite.

Characterization of experimental products

The run products were examined by optical microscopy, XRD, microprobe analysis and Mössbauer spectroscopy.

Routine XRD patterns were collected with an automated Siemens D-500 diffractometer (CuK_α radiation, 40 kV/30 mA, step size = 0.03 2Θ, counting time 1s per step). For unit cell refinements synthetic silicon ($a_0 = 5.43088$ Å) was added as internal standard and measuring conditions were modified to a step size of 0.01 2Θ and a counting time of 7 s, collected between 5 and 65° (2Θ). The refinements given in Table 2, obtained from annite in the mixture annite + sanidine + magnetite, were calculated with a modified version of the least squares program of Appleman and Evans (1973).

Table 2 Chemical composition (first part) and lattice constants (second part) of annite coexisting with sanidine + magnetite between 500 and 800° C and 2.8 kbar (*n* number of microprobe analyses). The formula units and mole fractions have been calculated as described in the text. X_{Ann}, X_{Ts}, X_{Fts} and X_{Vac} are the mole fractions of the annite-, Tschermakite, Ferri-Tschermakite and vacancy end members, as defined in the text. a^{id}_{Ann} is the ideal activity of annite (calculated as $a^{id}_{Ann} = 4X_K(X^{oc}_{Fe^{2+}})^3 X^{T2}_{Al} X^{T2}_{Si}$) (N.D. not determined). Numbers in parentheses are one standard deviation and refer to the last digit

Run number	EQ1C14		EQ1C17		EQ1C11-2		EQ1C16		EQ1C12		EQ1C15		EQ1C13	
T° C	500		550		600		650		700		750		800	
% Fe^{3+} [a]	14.3		ND		ND		ND		7.7		ND		12.4	
n	50		50		32		18		42		102		46	
SiO_2	33.8	(4)	33.8	(7)	33.5	(5)	32.9	(6)	33.0	(6)	32.3	(5)	31.9	(4)
Al_2O_3	12.0	(2)	10.9	(4)	11.3	(3)	12.6	(5)	11.8	(3)	13.4	(3)	12.7	(7)
FeO	39.5	(5)	38.3	(9)	38.0	(6)	38.5	(8)	41.0	(7)	40.2	(7)	39.6	(7)
K_2O	9.3	(2)	9.1	(3)	8.9	(3)	9.0	(3)	9.2	(2)	9.2	(2)	9.1	(2)
Si	2.87	(2)	2.94	(4)	2.92	(3)	2.83	(4)	2.81	(3)	2.74	(3)	2.76	(3)
Al^{IV}	1.13	(2)	1.06	(4)	1.08	(3)	1.17	(4)	1.17	(2)	1.26	(3)	1.24	(4)
Al^{VI}	0.07	(3)	0.06	(5)	0.08	(4)	0.11	(5)	0.02	(3)	0.08	(4)	0.06	(4)
Fe^{2+}	2.48	(6)	2.46	(9)	2.45	(6)	2.45	(9)	2.59	(8)	2.53	(8)	2.54	(6)
Fe^{3+}	0.32	(3)	0.32	(3)	0.32	(3)	0.32	(3)	0.34	(3)	0.33	(3)	0.33	(3)
K	1.01	(3)	1.01	(4)	0.99	(4)	0.99	(4)	1.00	(2)	0.99	(3)	1.00	(2)
X_{Ann}	0.83	(2)	0.82	(3)	0.81	(2)	0.82	(3)	0.85	(2)	0.84	(2)	0.85	(2)
X_{Ts}	0.02	(1)	0.02	(2)	0.03	(1)	0.04	(2)	0.01	(1)	0.03	(1)	0.02	(1)
X_{Fts}	0.02	(2)	0.00	(3)	0.00	(2)	0.02	(1)	0.05	(1)	0.06	(2)	0.06	(2)
X_{Vac}	0.13	(2)	0.16	(4)	0.16	(3)	0.13	(4)	0.09	(2)	0.07	(3)	0.08	(2)
a^{id}_{Ann}	0.55	(4)	0.55	(6)	0.54	(4)	0.53	(6)	0.61	(4)	0.56	(4)	0.57	(5)
a_0	5.388	(1)	5.391	(2)	5.392	(2)	5.393	(2)	5.396	(2)	5.399	(3)	5.405	(3)
b_0	9.339	(5)	9.337	(6)	9.339	(4)	9.330	(6)	9.340	(6)	9.341	(13)	9.324	(10)
c_0	10.311	(5)	10.317	(4)	10.316	(4)	10.320	(4)	10.319	(6)	10.326	(8)	10.315	(11)
β	100.13	(3)	100.13	(3)	100.09	(3)	100.13	(4)	100.07	(3)	100.18	(6)	100.19	(6)
$V_{[cm^3]}$	153.81	(11)	153.95	(13)	154.01	(11)	153.94	(3)	154.21	(14)	154.35	(25)	154.09	(25)

[a] Determined by Mössbauer spectroscopy

Due to a lot of overlapping reflections they are one order of magnitude less accurate than annite lattice parameters given by Redhammer et al. (1993), measured on "pure" annite.

For microprobe analyses small uncrushed parts of the experimental charge were pressed to flat disks, which then were deposited on glass slides (as commonly used in the preparation of thin sections) and then covered with carbon. This turned out to be a very simple and fast technique compared to polished samples, which are much more time consuming to prepare. The flat disks produced in that way had ± horizontal surfaces in the middle, and at least three different parts of that central area were selected for analysis (in sum around 50 analyses were gathered for each sample, in one case only 18, in another 102). To check the effect of possible systematic errors introduced in that way, a second polished sample was also measured (it was prepared from a run at 800° C showing a reaction mixture with recrystallized annite in large enough plates of ~2 μm in thickness). Because both types of samples yielded the same results within error limits, it is believed that systematic errors did not affect the microprobe data significantly. The WD-analyses were performed on a JEOL-JX 8600 microprobe and automatically ZAF-corrected. Operating conditions were 15 kV, 4.0 nA beam current, 10 s counting time with the beam focused to <1 μm. This seemed a reasonable compromise between counting statistics, which become better with increasing beam current, and the volume excited by the beam in the sample, which should be kept low, in order to avoid mixed analyses in the usually fine grained experimental products.

Mössbauer spectroscopy was performed on selected products in order to determine the Fe^{3+} contents of annite in the reaction mixture (Fig. 3 gives an example). Because there is no chance to separate the finely intergrown minerals after the run, the spectra are complicated by the fact that magnetite as another Fe^{2+}/Fe^{3+} phase is present, reducing the accuracy of the calculated Fe^{3+} content in annite to approximately ±2–3%. Due to overlapping absorptions with magnetite, the amount of tetrahedral Fe^{3+} could not be detected in the spectra and all Fe^{3+} is taken as octahedral. However, based on the work of Redhammer et al. (1993, Table 4a), the ratio $Fe^{3+}_{tet}/Fe^{3+}_{total}$ will probably not exceed ~0.25 in the present experiments. Details of the experimental design, operating conditions and fitting procedures are given in that paper and will not be repeated here.

Comparison of relative peak intensities on XRD scans served as a criterion in some classical oxygen buffered experiments to decide in which direction the reaction progressed.

Conventional f_{O_2} buffers

This is the commonly applied technique to locate f_{O_2}-dependent equilibria and was used in some experiments to try to reverse equilibrium (1) along the NNO and QFM buffer curves. For QFM, fayalite was synthesized from mixtures of quartz, Fe and Fe_2O_3 placed in evacuated quartz-glass tubes and held at 900° C for at least 12 hours. Due to the diffusion of H_2 through noble metals, the f_{O_2} of the buffer can be imposed on the sample by enclosing a $Ag_{70}Pd_{30}$ capsule containing the assemblage of the reaction to be studied $+H_2O$ into a larger Au tube filled with the buffer $+H_2O$. This method works the better the steeper the slope of an equilibrium is relative to that of the buffers.

Hydrogen-sensor technique

To monitor the f_{H_2} of equilibrium (1) between 500 and 800° C in 50° C intervals, the H_2-sensor technique, mainly used by Chou and coworkers, was employed. This method is based on the Ag-AgCl buffer (Chou and Eugster 1976),

$$Ag + HCl = AgCl + 1/2\,H_2, \quad (2)$$

whose equilibrium constant $K_2 = (a_{AgCl} \cdot f_{H_2}^{0.5})/(a_{Ag} \cdot f_{HCl})$ relates f_{H_2} to f_{HCl} and therefore also f_{H_2} to the concentration of HCl in the solution. In practice two sensors are used, one with an initial

HCl concentration lower and the second higher than the expected equilibrium value. The closeness of the final concentrations is then a measure for the attainment of equilibrium. The capsule configuration used is exactly the same as described by Chou (1987a). Approximately 20 mg solid Ag and AgCl together with 25 µl distilled water (sensor A) or HCl (sensor B) were sealed into Pt capsules of 18 mm × 1.8 mm (ID) × 2.3 mm (OD). Both sensors were then sealed into an Au tube of 35 mm × 4.8 mm (ID) × 5.3 mm (OD) with a stoichiometric mixture of annite + sanidine + magnetite (totalling in average 290 mg) and 20–25 mg H_2O. After the experiment, the sensor capsules were cleaned with a copper brush, weighed, and then punctured on a Teflon plate with a tungsten carbide needle. Under the binocular 3–4 aliquots of the HCl solution (each 5 µl) were picked up with a micropipette and then analysed with a Buchler chloridometer, which measures molarities of chloride (M_{Cl^-}). Each datum of the sensors A and B is included in Table 1, the mean value is labelled ($M^m_{Cl^-}$). The instrument was calibrated before with different HCl solutions of known concentrations, which were reproduced with satisfactory accuracy (errors of <1–2%, depending on concentration). In the next step, measured M_{Cl^-} was converted to molalities (m_{Cl^-}) using Eq. (3.23) of Chou (1987a), derived from density data for HCl solutions. Based on the work of Frantz and Marshall (1984) on the dissociation constants of HCl (see Chou 1987a, Table 3.5), the molality of associated HCl at P and T of the experiment, $(m_{HCl})_{P,T}$, relevant for the Ag-AgCl buffer, was computed next. These data show that HCl is mainly dissociated at 1 bar/298° C, but associated to nearly 100% at experimental conditions, if temperature is not too low (>500° C) and pressure not too high (<2 kbar).

Unfortunately, the equilibrium constant K_2 cannot be calculated from thermochemical data directly, but must be calibrated by a reference experiment in order to determine the desired f_{H_2} of the outer system from the measured HCl concentrations of the sensors. As explained by Chou (1987a), this leads to the relation (Chou 1987a, Eq. 3.26):

$$(f^S_{H_2})_{P,T} = (f^R_{H_2})_{P,T}\,(m^S_{HCl}/m^R_{HCl})^2_{P,T}, \tag{3}$$

where $(f^S_{H_2})_{P,T}$ is the fugacity of H_2 in the sample S to be measured at P and T, $(f^R_{H_2})_{P,T}$ is the fugacity of H_2 in the reference experiment R, performed at the same P–T conditions and with a buffer whose f_{H_2} (respectively f_{O_2}) is known as a function of P and T, and $(m^R_{HCl})_{P,T}$ and $(m^R_{HCl})_{P,T}$ are the molalities of associated HCl in the sample and reference at P and T as determined from the measured molarities at 1 bar/298° C, based on the relationship: $(m_{Cl^-})_{1/298} = (m_{Cl^-} + m_{HCl})_{P,T}$ (Chou 1987a, Eq. 3.16).

Nickel-nickel oxide was chosen as reference, because firstly its $\log f_{O_2} - T$ location is in the vicinity of the expected position for equilibrium (1), and secondly very accurate emf data are now available for this buffer (O'Neill 1987a). The NNO buffer was corrected to the experimental pressure using volumetric data for Ni and NiO of Robie et al. (1978). The f_{O_2} of the reference obtained in that way was then converted to f_{H_2} employing the activity model for H_2O–H_2 fluids of Grevel and Chatterjee (1992) and an iterative procedure based on the relation:

$$\frac{(K^{diss}_{H_2O})_{P,T}\,(f^0_{H_2O}\,a_{H_2O})_{P,T}}{(f^0_{H_2}\,a_{H_2})_{P,T}} = (f_{O_2})^{0.5}_{P,T} \tag{4}$$

For a given P, T and f_{O_2} (right hand side of Eq. (4), RHS), the left hand side (LHS) of (4) is as long iterated in X_{H_2}, as long LHS = RHS, from which follows $(f^R_{H_2})_{P,T} = f^0_{H_2}\,a_{H_2})_{P,T}$, as used in Eq. (3). The $(K^{diss}_{H_2O})_{P,T}$ was calculated from the TWEEQ data base (Berman 1991), consisting of the thermodynamic data of Berman (1988), supplemented by additional data (e.g. for H_2 and O_2).

Calculation of structural formulae

Structural formulae of annite given in Table 2 have been calculated assuming a Fe^{3+} content in all annites of 11.5% (the mean of the Mössbauer data). Based on the evidence discussed before, Fe^{3+} is preferentially incorporated by a vacancy-coupled substitution rather than the oxyannite substitution. The formulae were therefore normalized to 11 oxygens and not to 8 cations and the calculation was done iteratively, stepwise increasing wt% Fe_2O_3 to a value so that the demanded 11.5% Fe^{3+} was reached. A Monte Carlo technique, as described by Kohn and Spear (1991), was used to process the analyses (between 18 and 102 from each run) and to estimate the standard deviations given in Table 2.

To express the formula units as mole fractions of biotite endmembers, the following end members were chosen: annite ($KFe^{2+}_3(OH)_2AlSi_3O_{10}$), a theoretical Tschermakite (Ts) endmember ($KAl_3(OH)_2AlAl_3O_{10}$), a theoretical Ferri-Tschermakite (Fts) endmember ($KFe^{3+}_3(OH)_2AlAl_3O_{10}$), and a vacancy (Vac) endmember with the formula ($KFe^{3+M2}_2Vac^{M1}(OH)_2AlSi_3O_{10}$). First, X_{Ts} was calculated by consuming all Al^{VI}. Next, as much X_{Fts} was computed as necessary to bring the Si/Al ratio to the ideal ratio of 3/1. The rest of Fe^{3+} remaining was then used up to build the vacancy endmember and all further remnants went into annite.

Thermodynamic calculations

At equilibrium, we have for reaction (1):

$$0 = \Delta H^0_R - T\Delta S^0_R + \int_{298}^{T} \Delta cp_R\,dT - T\int_{298}^{T} (\Delta cp_R/T)\,dT + \int_1^P \Delta V_s\,dP + RT\ln K, \tag{5}$$

where $K = (f_{H_2}/a_{ann})$ with f_{H_2} given in Table 1 and a_{ann} in Table 2. The activity model used, accounting for the incorporation of the determined amounts of Fe^{3+} and for the deviation of annite chemistry from the ideal (id) Si/Al ratio, is: $a^{id}_{Ann} = 4X_K(X^{oc}_{Fe^{2+}})^3 \cdot X^{T2}_{Al}X^{T2}_{Si}$ (e.g. Holland and Powell 1990). This ideal model implies mixing on three octahedral sites and assumes that the oxyannite substitution can be neglected. These assumptions seem reasonable in the light of the evidence presented by Redhammer et al. (1993) and references cited therein, showing that mixing occurs on all three M sites, with a slight preference of Fe^{3+} and vacancies to occupy the M1 site, and that the oxyannite substitution is probably not of major importance. In the tetrahedral sheet this model implies a long-range ordered distribution, where Al and Si mix only on the T2 sites. The effect of using an alternate model representing complete short range order ($a_{ann} = X_{ann}$) on the derived standard-state properties of annite, was also tested. Combining the last four terms as K^*, we can transform (5) to the form:

$$\ln K^* = -(\Delta H^0_R/R)\,1/T + \Delta S^0_R/R, \tag{6}$$

showing that in a plot of lnK* versus 1/T (Fig. 1) the experimental half-brackets should lie on opposite sides of a line, whose slope defines $-\Delta H^0_R/R$ and whose intercept is $\Delta S^0_R/R$. To calculate K* from the equilibrium data, all other thermodynamic data necessary (including λ-transition terms for magnetite) were taken from the TWEEQ data base (Berman 1991) and combined with the experimentally determined values for $K = (f_{H_2}/a_{ann})$. The unit cell refinements of sanidine from the experimental runs show that it is completely disordered high sanidine. Consequently the thermodynamic data of that phase had to be used in the calculations (except for runs performed at 500 and 550° C, where it starts to order slightly and where the data of K feldspar together with order/disorder terms, as given by Berman, 1988, have been used instead). To obtain ΔH^0_R

and ΔS_R^0, a least squares technique was employed, which in matrix notation can be written as (e.g. Powell and Holland 1985; Holland and Powell 1985, 1990):

$$p = (K^T . W_d^2 . K)^{-1} . (K^T . W_d^2 . d), \tag{7}$$

where p is the vector containing the fitted parameters (ΔH_R^0 and ΔS_R^0), K is the matrix of coefficients of the least squares problem, d is the data-vector given by the LHS of (6), and W_d is a weighting matrix of the lnK* data (a diagonal matrix with elements $1/\sigma_{d,i}$). From the regressed ΔH_R^0 and ΔS_R^0, annite standard-state properties were then calculated from the relations:

$$H^0_{f,\mathrm{Ann}} = H^0_{f,\mathrm{San}} + H^0_{f,\mathrm{Mag}} + H^0_{f,\mathrm{H_2}} - \Delta H^0_R, \text{ and} \tag{8}$$

$$S^0_{\mathrm{Ann}} = S^0_{\mathrm{San}} + S^0_{\mathrm{Mag}} + S^0_{\mathrm{H_2}} - \Delta S^0_R. \tag{9}$$

Error propagation

In order to establish the W_d matrix necessary in Eq. (7), the standard error propagation formalism was applied. It states that if Y is a function of several variables, $Y = f(x_1, \ldots, x_n)$, then the variance of Y, σ_Y^2, is given by:

$$\sigma_Y^2 = \sum_{i=1}^{n} \sum_{j=1}^{n} \sigma_{x_i x_j} (\partial Y/\partial x_i)(\partial Y/\partial x_j), \tag{10}$$

where $\sigma_{x_i x_j}$ denotes the covariance between x_i and x_j, $(\partial Y/\partial x_i)$ and $(\partial Y/\partial x_j)$ are the partial derivatives of Y with respect to x_i and x_j. An estimate of the uncertainties on the regressed parameters is immediately available through the covariance matrix V_d:

$$V_d = (K^T . W_d^2 . K)^{-1} \sigma_r^2 \tag{11}$$

where σ_r^2 is the mean square of residuals given by:

$$\sigma_r^2 = (r^T . r)/(n - m) \text{ with } r = W_d . (d - K . p), \tag{12}$$

where n is the number of data available and m is the number of parameters fitted (two in this case).

Based on Eq. (10) applied to Eq. (3), the standard deviation of the equilibrium $f_{\mathrm{H_2}}$ was calculated in a first step (Table 1), by propagating the σ of $(M_{Cl^-})^m$ of sample and reference as well as the relatively small σ of $f^R_{\mathrm{H_2}}$, estimated by using errors given in O'Neill (1987a) on μ_{O_2} converted to $\sigma_{f_{\mathrm{H_2}R}}$. Applying Eq. (10), $\sigma_{f_{\mathrm{H_2}S}}$ is calculated from:

$$\begin{aligned}\sigma_{f^S_{\mathrm{H_2}}} = [&(\sigma_{m^S_{\mathrm{HCl}}})^2 (2 f^R_{\mathrm{H_2}} m^S_{\mathrm{HCl}}/(m^R_{\mathrm{HCl}})^2)^2 \\ &+ (\sigma_{m^R_{\mathrm{HCl}}})^2 (-2 f^R_{\mathrm{H_2}} (m^S_{\mathrm{HCl}})^2/(m^R_{\mathrm{HCl}})^3)^2 \\ &+ (\sigma_{f^S_{\mathrm{H_2}}})^2 (m^S_{\mathrm{HCl}}/(m^R_{\mathrm{HCl}})^2]^{1/2}.\end{aligned} \tag{13}$$

σ^*_{lnK} was then calculated by further error propagation including additional errors in T of 5° C, in P of 50 bar, and in a_{ann}, as given in Table 2, for each datum.

An error of 0.1% in H_f^0 and of 1% in S^0 of the phases sanidine, magnetite and H_2 has been assumed for the tabulated values in the calculation of the final errors in $H^0_{f,\mathrm{Ann}}$ and S^0_{Ann}. All calculations were done with the program *Mathematica* (Wolfram Research Inc. 1993).

Results

Hydrogen-sensor data

The hydrogen-sensor data are compiled in Table 1 and shown in Fig. 1 including $\pm 2\sigma$ error bars, together with all oxygen buffer brackets. To test the reproducibility of the results, experiments were repeated once at 600° C and 700° C and twice at 750° C, indicating that precision around 0.05 $\log f_{O_2}$ units at 600° C decreases to ~ 0.2 $\log f_{O_2}$ units at 750° C. Depending on the $f_{\mathrm{H_2}}$-environment around the gold capsule in relation to the internal $f_{\mathrm{H_2}}$ as produced by the annite + sanidine + magnetite mixture, the relative proportions of these three minerals changed in some experiments. The solid line fitted through the sensor data (the adjacent broken lines are the $\pm 1\sigma$ uncertainty envelope) defines a ΔH_R^0 of 50.269 ± 3.987 kJ/mol and a ΔS_R^0 of 83.01 ± 4.35 J/(K.mol) for equilibrium (1) with a correlation coefficient $\rho = 0.995$.

The mineralchemical data obtained for annite (Table 2, Fig. 2a) indicate the rough trend of decreasing Si pfu with temperature (from ~ 2.9 at low to ~ 2.75 at high temperatures), Al^{total} behaves inversely, so the annites show the tendency to become slightly richer in Al with increasing temperature. This change in annite composition explains why in the high temperature runs (above 650° C) fayalite was found in increasing

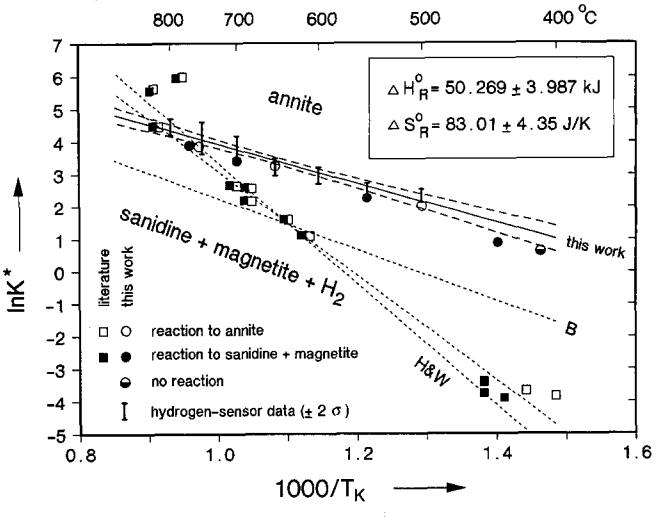

Fig. 1 Experimental data for the reaction annite = sanidine + magnetite + H_2, plotted as lnK*, as defined in the text, versus $1000/T_K$. The hydrogen-sensor data of this study (Table 1) are shown including $\pm 2\sigma$ error bars. The *squares* represent classical oxygen buffer brackets from sources given in Table 3, the *solid line* is the least squares fit to the hydrogen-sensor data, the adjacent *stippled lines* are the corresponding 1σ-uncertainty envelope. Values of ΔH_R^0 and ΔS_R^0 resulting from this fit are given in the figure. The *parallel dotted line* labelled *B* is the position of reaction (1) based on the thermodynamic data set of Berman, the *steeper line* labelled *H* and *W* was calculated according to Hewitt and Wones (1984). For further explanations see text

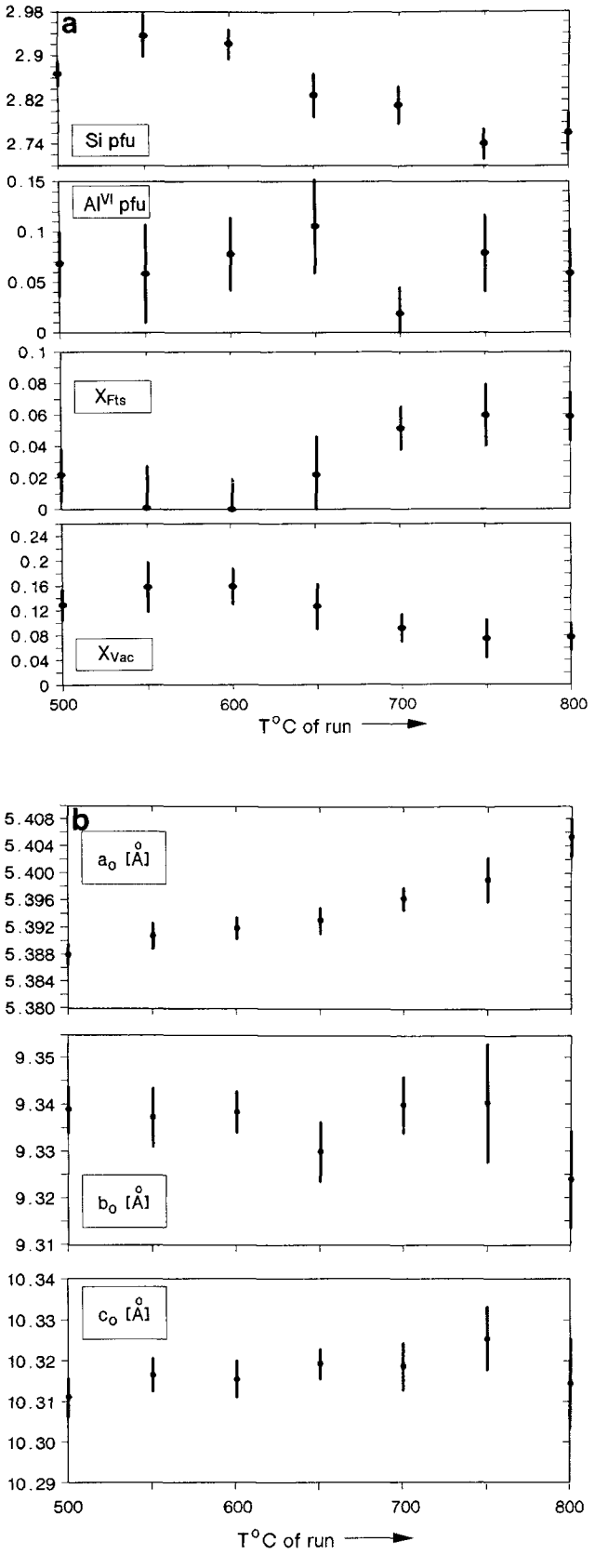

amounts of maximal ~ 10% at 800° C. The Al^{VI} remains approximately constant averaging 0.07 ± 0.03 pfu, consequently the same applies for $X_{Ts} = 0.02 \pm 0.01$. Following from the calculation procedure of endmembers, the observed trend for Al and Si is reflected by X_{Fts} (increasing from values close to 0 to ~ 0.06 with temperature) and by X_{Vac} respectively (decreasing from ~ 0.15 to ~ 0.08 with temperature). The X_{Ann} averages to 0.83 ± 0.014 in all annites, the ideal activity a^{id}_{Ann} to 0.56 ± 0.02, calculated from the site fractions according to Holland and Powell (1990). In the unit cell data (Fig. 2b) a clear trend is only visible for a_0, which increases with temperature.

The microprobe analyses of sanidine indicate that this phase deviates insignificantly from its ideal composition by incorporation of 0.8 wt% FeO at maximum. In some runs, where the mixture reacted to produce sanidine + magnetite, magnetite crystals were large enough to be analysed, showing that only negligible amounts of the hercynite component are present.

Solid oxygen buffer brackets

To check the hydrogen-sensor (HS) data obtained by another method, the conventional oxygen buffer technique was applied to get brackets along the QFM and NNO buffers (Table 3, Fig. 1). For QFM a relatively close bracket was located at 755 and 770° C and 4.2 kbar, which is in agreement with the HS data within error limits. Along the NNO buffer experiments performed at 2.8 kbar lasting 980 h are also compatible with the HS data. They show clear sign of reaction to sanidine + magnetite at 440° C, whereas at 410° C no discernible reaction occurred after that time. Experiments at still lower temperatures seemed not reasonable. Further constraints incorporated in Table 3 and Fig. 1 come from synthesis experiments of Redhammer et al. (1993). These data show that at 6 kbar reaction (1) should intersect QFM between 650 and 700° C and NNO between 500 and 550° C, which is also in concordance within errors with the $\log f_{O_2}$-T position of equilibrium (1) as determined by the HS technique.

Fig. 2 **a** Mineral chemistry of annites in equilibrium with sanidine + magnetite, as measured in the experimental runs performed between 500 and 800° C. Plotted data are from Table 2: Si per formula unit (pfu), Al^{VI} pfu, mole fraction of the Ferri–Tschermak's component (X_{Fts}), and mole fraction of the vacancy endmember (X_{Vac}), both as defined in the text. **b** Lattice constants (a_0, b_0 and c_0) of annites in equilibrium with sanidine + magnetite, as measured in the experimental runs performed between 500 and 800° C

Table 3 Experimental oxygen buffer data (half-brackets) available for the equilibrium annite = sanidine + magnetite + H_2. Buffers *HM* hematite-magnetite, *NNO* nickel-nickel oxide, *QFM* quartz-fayalite-magnetite, *MW* magnetite-wuestite, G-CH graphite-methane $\log f_{O_2}$ of NNO, QFM and MW was calculated on the basis of emf measurements of O'Neill (1987a, b and 1988), $\log f_{O_2}$ of HM was computed using the thermodynamic data of Berman (1988), $\log f_{H_2}$ of G-CH is given according to Chou (1987b). The conversion $\log f_{O_2} \langle\!\rightarrow\!\rangle \log f_{H_2}$ was done as described in the text. lnK* is a modified equilibrium constant, combining $\ln f_{H_2}$ with all thermodynamic terms except ΔH_R^0 and ΔS_R^0 (see text). (*E&W* Eugster and Wones 1962, *R* Rutherford 1969, *H&W* Hewitt and Wones 1984, R et al. Redhammer et al. 1993)

Run Number	*P* [kbar]	*T* [°C]	Buffer	Duration	$-\log f_{O_2}$	$\log f_{H_2}$	Starting material	Result	Interpretation	$\ln^{K*}$	Reference
672	2.07	400	HM	3072	23.815	−1.786	A[a]	A, H, S	?←	−3.775	E & W
1537	2.07	450	HM	960	21.331	−1.570	A	A, S, M, H	→	−3.320	E & W
1527	2.07	635	NNO	144	17.990	0.710	S, M	A, S, M	←	1.675	E & W
1482	2.07	640	NNO	328	17.842	0.719	S, M	S, M	→	1.691	E & W
1505	2.07	700	QFM	227	16.931	1.196	S, M	A, S, M	←	2.720	E & W
1511	2.07	710	QFM	209	16.673	1.212	A	A, S, M	→	2.746	E & W
927	2.07	820	MW	70	16.909	2.683	F, L, K	F, S, A	←	6.057	E & W
1590	2.07	830	MW	166	16.640	2.664	A	S, M, A	→	6.008	E & W
980	1.035	435	HM	360	22.063	−1.812	S, M	S, M	→	−3.834	E & W
983	1.035	450	HM	360	21.360	−1.750	A	A, M, H, S	→	−3.704	E & W
1533	1.035	610	NNO	160	18.809	0.462	S, M	A, S, M	←	1.164	E & W
1529	1.035	620	NNO	163	18.497	0.480	A	A, S, M	→	1.190	E & W
1534	1.035	680	QFM	160	17.567	0.974	S, M	A, S, M	←	2.252	E & W
1536	1.035	690	QFM	162	17.296	0.986	A	S, M	→	2.269	E & W
954	1.035	780	MW	96	18.120	2.504	S, M	A, S, M	←	5.687	E & W
643	1.035	790	MW	90	17.831	2.484	A	A, S, M	→	5.634	E & W
187	2.0	680	QFM	408	17.472	1.156	M, S, Q, F	M, S, A, Q	←	2.650	R
128A	2.0	689	QFM	144	17.229	1.17	A	M, S, A	→	2.672	R
102A	2.0	828	G-CH	24	15.349	2.019	M, S	A, M, S	←	4.525	R
127	2.0	834	G-CH	48	15.231	2.027	A	A, F, L	→	4.541	R
Fig. 10	2.0	420	HM		22.774	−1.710			←	−3.613	H & W
Fig. 10	2.0	450	HM		21.333	−1.581			→	−3.344	H & W
EQ1#8B	2.8	410	NNO	980	26.865	0.171	A, S, M	A, S, M	=	0.702	This work
EQ1#8A	2.8	440	NNO	980	25.349	0.286	A, S, M	−A, +S, M	=→	0.942	This work
EQ1#7	4.2	755	QFM	669	15.879[b]	1.760	A, S, M	+A, −S, M	←	3.927	This work
EQ1#8	4.2	770	QFM	504	15.536[b]	1.781	A, S, M	−A, +S, M	→	3.966	This work
A37	6.0	500	NNO	768	22.483	0.848	A	A	←	2.087	R et. al.
A42	6.0	550	NNO	148	20.565	0.983	A	A, M, S	→	2.335	R et al.
A29	6.0	650	QFM	668	17.912	1.478	A gel	A, (F, S)	←	3.336	R et al.
A13	6.0	700	QFM	860	16.553	1.566	A gel	A, S, M	→	3.486	R et al.

[a] *A* annite, *S* sanidine, *M* magnetite, *H* hematite, *Q* quartz, *F* fayalite, *L* leucite, *K* kalsilite, + indicates increase, − decrease; → reaction to sanidine + magnetite + H_2; ← reaction to annite; = no reaction

[b] Corrected by −0.5 following from hydrogen-sensor measurements

Comparison with existing oxygen buffer brackets

If older reversals of equilibrium (1) are compared to the combined HS and oxygen buffer data of this study, it turns out that agreement exists only at high temperatures (Fig. 1), whereas pronounced differences appear at low temperatures. Most of the previous data came from Eugster and Wones (1962). Considering their results obtained at 2.07 and 1.035 kbar, self-consistency seems fullfilled for their HM, NNO and QFM brackets, whereas the two MW reversals lie clearly aside from the general trend as indicated by the other buffers. The half-brackets of Rutherford (1969) at the QFM and G-CH buffers, and of Hewitt and Wones (1984) at HM fit well to the pattern of the Eugster and Wones data. In comparison to the data presented here, only the G-CH bracket of Rutherford is in perfect agreement, all other brackets are not, with the largest discrepances observed for the HM reversals. If all the oxygen buffers brackets except those for MW are used in a regression analysis (Fig. 1, steep dotted unlabelled line), ΔH_R^0 would amount to 134.089 ± 3.441 kJ/mol and ΔS_R^0 to 160.035 ± 3.993 J/(K.mol). For comparison the relation $\log f_{H_2} = -8113/T + 9.59 + 0.0042\ (P-1)/T$, as given by Hewitt and Wones (1984) for equilibrium (1), converted to logarithmic scale, is also shown in Fig. 1 (labelled H&W).

Standard-state properties of annite

Utilizing a refined set of unit cell data of annites synthesized at different $\log f_{O_2}$-T conditions (Redhammer

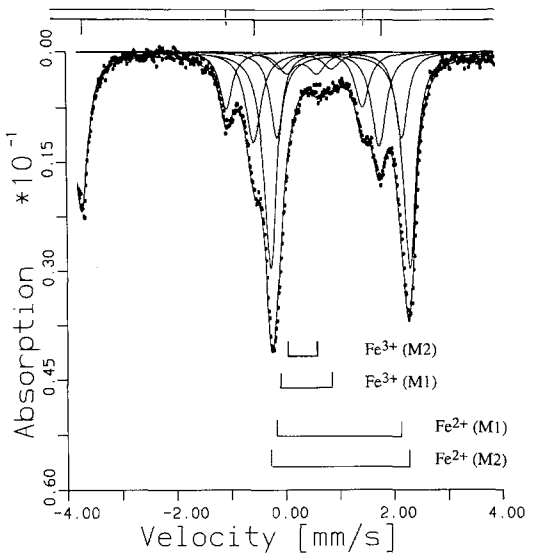

Fig. 3 Mössbauer spectrum of annite coexisting with sanidine + magnetite (run EQ1C14, 500° C). The derived Fe^{3+} content in this case is 14.3%

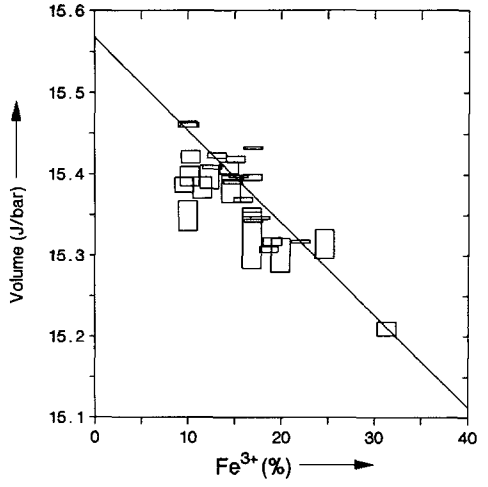

Fig. 4 Plot of the molar volume of annite versus its Fe^{3+} contents, as determined by Mössbauer spectroscopy. Data are from Redhammer et al. (1993, Table 3). The least squares fit to these data (*solid line*) gives a molar volume of 15.568 ± 0.030 (J/bar) for pure annite

et al. 1993, Table 3), and extrapolating volumes back to 0% Fe^{3+}, (Fig. 4), the molar volume of annite is constrained as 15.568 ± 0.030 J/bar ($\rho = -0.984$). This value is somewhat higher than published volumetric data of annite, because these ignore the effect of Fe^{3+}.

Based on the least squares derived values of $\Delta H^0_R = 50.269 \pm 3.987$ kJ/mol and $\Delta S^0_R = 83.01 \pm 4.35$ J/(K.mol) for equilibrium (1) and on the thermodynamic data for sanidine, magnetite and H_2 of Berman (1988, and TWEEQ data base), the standard-state properties of annite are: $H^0_{f,\mathrm{Ann}} = -5127376 \pm 5729$ J/mol and $S^0_{\mathrm{Ann}} = 422.84 \pm 5.29$ J/(K mol) (these values change slightly to $H^0_{f,\mathrm{Ann}} = -5128039 \pm 6105$ J/mol and $S^0_{\mathrm{Ann}} = 425.49 \pm 5.80$ J/(K mol), if the alternate activity model, $a_{\mathrm{ann}} = X_{\mathrm{ann}}$, is used). Compared to literature data, (Table 4), which have been derived mainly from the Fe-Mg partitioning experiments of Ferry and Spear (1978) so far, using different assumptions on the activities of garnet and biotite, the properties derived here are rather similar for S^0_{Ann} and lower by ~ 15 kJ for $H^0_{f,\mathrm{Ann}}$, underlining the validity of the $\log f_{O_2}$-T location of equilibrium (1), as determined in this study. Considerably different standard-state properties, namely $H^0_{f,\mathrm{Ann}} = -5211195 \pm 5364$ J/mol and $S^0_{\mathrm{Ann}} = 345.81 \pm 5.00$ J/(Kmol), would result on the other hand from the published oxygen buffer data.

Figure 5a depicts the revised stability field of annite, calculated for the experimental pressure of 2.8 kbar between 400 and 800° C (Fig. 5a, vertically rules area). In marked contrast to the position of equilibrium (1) as computed from published oxygen buffer reversals (Fig. 5a, dotted line), intersecting with HM, NNO and QFM at points labelled E, N and D according to Eugster and Wones (1962, their Fig. 4), the calculated curve based on the HS data of this study intersects only with QFM around 510° C. The lower stability boundary of annite in terms of $\log f_{O_2}$ is given by the reaction:

$$\text{annite} + 3H_2 = \text{sanidine} + 3\ \text{iron} + 4H_2O. \quad (14)$$

The calculated position of this equilibrium is rather close to the IQF (iron-quartz-feyelite) buffer curve, which it intersects at very low angle somewhat below 400° C. The relevant equilibria, which close the annite stability field at $T > 800$° C are schematically shown in Fig. 5b. They involve leucite and kalsilite as additional K bearing phases. The T-X_{H_2}, T-$\log f_{H_2}$ and T-$\log f_{O_2}$ relations of all reactions and isobaric invariant points confining annite stability, calculated between pressures of 1 and 5 kbar, will be given in a separate paper.

Discussion

The hydrogen-sensor technique was the main method applied in this study to locate the $\log f_{O_2}$-T position of the redox reaction annite = sanidine + magnetite + H_2. The equilibrium data, obtained from 500 to 800° C in 50° C intervals, have been used to retrieve the standard-state properties of annite consistent with the thermodynamic data base of Berman (1988, 1990, TWEEQ). Values of $H^0_{f,\mathrm{Ann}}$ and S^0_{Ann} were found to be -5127376 ± 5729 J/mol and 422.84 ± 5.29 J/(K mol), respectively. This $H^0_{f,\mathrm{Ann}}$ is somewhat lower than former results, the extracted S^0_{Ann} agrees within error limits with previous determinations based on experimental Fe-Mg exchange data between garnet and biotite (Berman 1990, Holland and Powell 1990) and on the exchange reaction phlogopite + 3FeO = annite + 3MgO (McMullin et al. 1991). The experimentally

Table 4 Comparison of annite standard-state properties from various studies (ND not determined)

Study	H_f^0 [kJ/mol]	S^0 [J/(K mol)]	V^0 [J/bar]
Eugster and Wones (1962)	−5167.24	N.D.	15.404 run $AnFe_8$
Berman (1990)[a]	−5142.800	420.000	15.408
Holland and Powell (1990)	−5149.320[b]	414.000	15.432
McMullin et al. (1991)	−5142.000[c]	421.01[d]	15.483[e]
This study	−5127.376 ± 5.729	422.84 ± 5.29	15.568 ± 0.030

[a] Properties derived from garnet-biotite data of Ferry and Spear (1978) in conjunction with the assumption of ideal mixing in biotite and the garnet activity model of Berman (1990)
[b] Derived from garnet-biotite data of Ferry and Spear (1978) and pyroxene-biotite data of Fonarev and Konilov (1986) in conjunction with the assumption of ideal mixing in all minerals
[c] Derived from experimental data and data of natural assemblages
[d] Estimated from the exchange reaction phlogopite + 3 FeO = annite + 3 MgO
[e] Taken from Hewitt and Wones (1975)

determined slope of equilibrium (1) is very close to that calculated from the internally consistent thermodynamic data base of Berman (Fig. 1, dotted line labelled B), a strong argument for the correctness of the $\log f_{O_2}$-T position of equilibrium (1) as inferred from the HS data of this study. These data were found also to be consistent with some half-brackets obtained by the classical oxygen buffer technique, but turned out to be compatible with published oxygen buffer brackets for reaction (1) only at high temperatures, whereas marked discrepances occur at lower temperatures. The reason for the lack of agreement in Fig. 1 could be one or more of the following three points:

1. Differences in the mineral chemistry of annites in the various experimental studies: If annite were strictly stoichiometric, reaction (1) would be univariant in $\log f_{O_2}$-T dimensions and $KAlSi_3O_8$, Fe, O_2 and H_2 could be chosen as components in this system. However, as demonstrated by the microprobe and Mössbauer data, annite deviates from its ideal composition and mole fractions of the vacancy and the Ferri–Tschermak's endmember become significant. These substitutions can be described by the two following reactions:

(A) $KFe_3^{2+}(OH)_2AlSi_3O_{10} + 2/3O_2 =$

$KFe_2^{3+}Vac(OH)_2AlSi_3O_{10} + 1/3Fe_3O_4$

(B) $KFe_3^{2+}(OH)_2AlSi_3O_{10} + 3/4O_2 + 3/2Al_2O_3 =$

$KFe_3^{3+}(OH)_2Al_4O_{10} + 3SiO_2,$

showing that for these substitutions, underlying f_{O_2}, there is also a dependence on the activities of Fe_3O_4, Al_2O_3 and SiO_2, and high activities of Fe_3O_4 and/or SiO_2 will stabilize the annite compound, lowering the Fe^{3+} content to its minimum value around 11%, as probably happened in the present experiments. Earlier experiments (especially the HM buffered ones) very likely determined the breakdown of higher Fe^{3+} annites, which could be caused by low activities of Fe_3O_4 and/or SiO_2 in these runs. This is supported by the trend of unit cell dimensions of annites in the experiments of Eugster and Wones (1962, Table 4), indicating varying Fe^{3+} in their annites. Based on the correlations of Fe^{3+} content with lattice constants of annite as given by Redhammer et al. (1993, Fig. 1), it appears that annites in the experiments of Eugster and Wones had the highest Fe^{3+} contents at HM buffered conditions, decreasing successively to the minimum value when equilibrated with the NNO, QFM and WM buffers and therefore the noted discrepancy of their equilibrium data to those presented in this study also decreases in the above order.

A combined form of substitutions (A) and (B), for example

(AoB)

$$KFe_{2.8}^{2+}Fe_{0.2}^{3+}(OH)_2Al_{1.2}Si_{2.8}O_{10} + 0.2SiO_2 + 0.15O_2 =$$

$$Fe_{2.1}^{2+}Fe_{0.6}^{3+}Vac_{0.3}(OH)_2AlSi_3O_{10} + 0.1Al_2O_3 + 0.1Fe_3O_4$$

could also explain why in the experiments of Redhammer et al. (1993, probably low activities of Al_2O_3 and Fe_3O_4) annites annealed near the upper $\log f_{O_2}$ boundary could have higher Fe^{3+} contents (around 19%, Si/Al close to 3/1), whereas annites coexisting with sanidine + magnetite are at their minimum Fe^{3+} at similar $\log f_{O_2}$ conditions and deviate more from the ideal Si/Al ratio.

2. Difficulties in assessing the reaction direction: To determine a reversal with the conventional oxygen buffer technique, the reaction direction must be identified. This is usually done by comparing relative intensities on XRD scans in combination with optical microscopy. If recrystallisation effects are significant in the experimental charge, a correct interpretation will be hampered. Additionally, if during cooling of the run a quench phase precipitates in amounts high enough to affect XRD patterns, this can also lead to a wrong

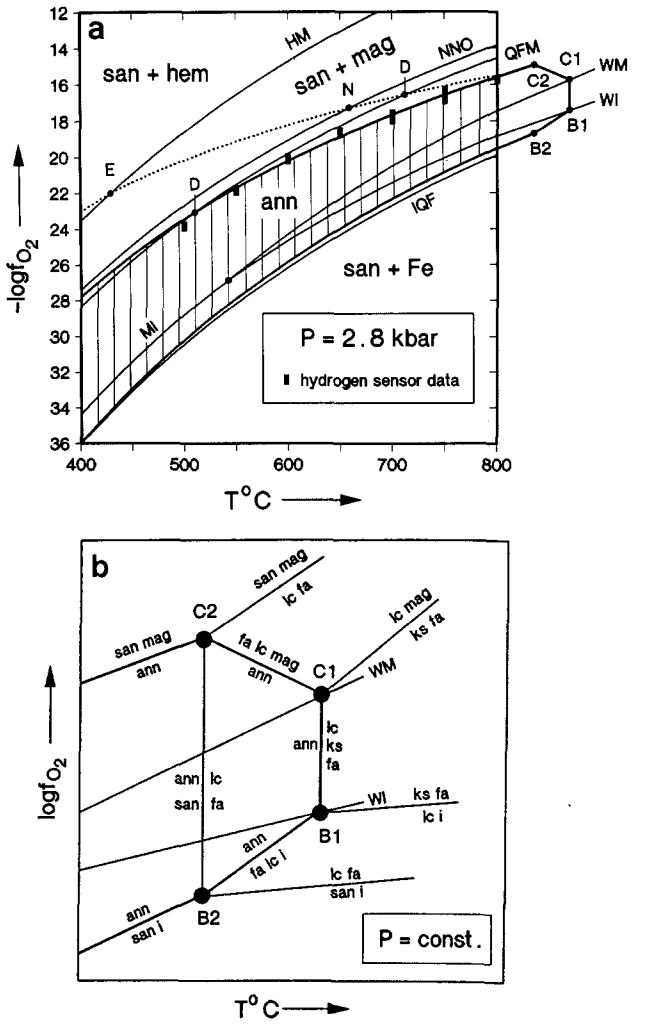

Fig. 5a Calculated stability field of annite at 2.8 kbar between 400 and 800° C (*vertically ruled area*). The upper and lower $\log f_{O_2}$-T stability limits (*heavy solid lines*) were computed with the annite standard-state properties as derived in this study (using $a_{ann} = 0.56$), and standard-state properties for the other phases from Berman (1988, and TWEEQ data base) in combination with H_2O-H_2 fluid activities resulting from the model of Grevel and Chatterjee (1992). The experimental $\log f_{O_2}$-T positions of the hydrogen-sensor data (Table 1) are shown for comparison. The height of the symbols represents $\pm 1\sigma$. The *stippled line* is the calculated positions of equilibrium (1) based on published O buffer brackets as compiled in Table 3 and plotted in Fig. 1 (it intersects with QFM, NNO and HM in points D, N and E labelled analogous to Eugster and Wones, 1962, their Fig. 4). The NNO, QFM, IQF and WM buffer curves are shown according to O'Neill (1987a, b, 1988); MI and WI buffers were calculated according to Chou (1987a, Table 3.1., least squares fit to unpublished data of Haas); HM was computed from the thermodynamic data of Berman (1988). The edge of the annite stability field above 800° C is only schematically outlined. **b** Details of that area around invariant points C2, C1, B1 and B2 and some reactions involved (*ann* annite, *san* sanidine, *hem* hematite, *mag* magnetite, *fa* fayalite, *i* iron, *lc* leucite, *ks* kalsilite)

interpretation of the reaction direction. The last possibility was considered by Rutherford (1969) to explain discrepances between his QFM results and those of Eugster and Wones (1962) on equilibrium (1). He concludes that Eugster and Wones in this case "apparently identified quench biotite as proof of biotite stability" (Rutherford 1969, p. 390).

3. Reasons related to kinetics: A remarkable feature of the oxygen buffer experiments is the fact that those performed with a mixture of annite + sanidine + magnetite obviously are in agreement with the HS data (the same is valid for the annealing experiments using gels as starting materials). On the other hand, the mixtures used in the older experiments were either annite or sanidine + magnetite alone. If there were a nucleation barrier for sanidine or magnetite necessitating some degree of overstepping of the equilibrium boundary in terms of temperature, this would systematically shift the half-brackets identifying first growth of sanidine + magnetite from annite to higher temperatures than the equilibrium value. This effect will be specially important for reactions intersecting at low angles with oxygen buffer curves like equilibrium (1) and will be the more pronounced the lower the temperatures. Of course, it does not explain the other type of half-brackets, which found annite in experiments started with sanidine + magnetite. Because reaction (1) and adjacent oxygen buffer curves have similar slopes, equilibrium (1) is in principle not a good candidate to be studied by the conventional oxygen buffer technique. As shown by Moecher and Chou (1990) the oxygen buffers are still a good method for locating equilibria with slopes diverse from those of the buffer curves, but obviously inferior compared to the HS technique in the present case.

Misfunction of oxygen buffers or of the HS technique is on the other hand not believed to be relevant for the discrepancy of the equilibrium data. For the oxygen buffers, the question may arise as to whether, at low temperatures (< 500° C as with HM) and hence slower diffusion kinetics of H_2, the experimental charge is successfully buffered to the appropriate value even at long run times. To clarify this point, calculations with Eq. (3.2.) of Chou (1987a) have been performed for some of the buffers and their f_{H_2} conditions as given in Table 3. This equation describes the permeation rate of hydrogen through a capsule as function of temperature, permeation constant of H_2 through precious metals (Chou 1987a, Table 3.3), capsule geometry, wall thickness and difference between internal and external f_{H_2}. The computations indicate that f_{H_2} gradients between charge and buffer can not persist for periods longer than some tens of minutes at maximum, even if the external f_{H_2} is defined by the HM buffer and temperature is low (assumptions made were: capsule material, $Ag_{70}Pd_{30}$; length, 2 cm; outer diameter, 0.35 cm; wall thickness, 0.25 mm; ideal fluid behaviour; internal f_{H_2} at the beginning = 0; 5–25 mg H_2O present; no H_2 loss by reaction, which corresponds to an experiment where the reaction in the charge is sluggish). For the HS technique, Chou (1987a, p. 81, and references therein) has demonstrated that equilibrium is approached

within a few days, which will also apply for the HS experiments of this study because of the similar experimental configuration (capsule dimensions, volumes of solutions).

Acknowledgements I want to thank L. Cemic for valuable comments on an earlier version of this paper, as well as A. Benisek for help during microprobe work and G. Redhammer for fitting the Mössbauer spectra. Further thanks are expressed to M. Grevel for supplying the Fortran source code of his program FLUIDTAB. The manuscript was improved by reviews of H.St.C. O'Neill and H. Annersten. Financial support by the Fonds zur Förderung der wissenschaftlichen Forschung (FWF), Austria, project P8392 CHE, is gratefully acknowledged.

References

Appleman DE, Evans HT (1973) Indexing and least-squares refinements of powder diffraction data. US Geol Surv Comput Contrib 20

Berman RG (1988) Internally consistent thermodynamic data for stoichiometric minerals in the system Na_2O-K_2O-CaO-MgO-FeO-Fe_2O_3-Al_2O_3-SiO_2-TiO_2-H_2O-CO_2. J Petrol 29:445–522

Berman RG (1990) Mixing properties of Ca-Mg-Fe-Mn garnets. Am Mineral 75:328–344

Berman RG (1991) Thermobarometry using multi-equilibrium calculations: a new technique, with petrological applications. Can Mineral 29:833–855

Chou IM (1987a) Oxygen buffer and hydrogen-sensor techniques at elevated pressures and temperatures. In: Ulmer GC, Barnes HL (eds) Hydrothermal experimental techniques. John Wiley and Sons, New York, pp. 61–100

Chou IM (1987b) Calibration of the graphite-methane buffer using f_{H_2} sensors at 2 kbar pressure. Am Mineral 72:76–81

Chou IM, Eugster HP (1976) A sensor for hydrogen fugacities at elevated P and T and applications. Trans Am Geophys Union 57:340

Eugster HP (1957) Heterogeneous reactions involving oxidation and reduction at high pressures and temperatures. J Chem Phys 26:1160

Eugster HP (1959) Reduction and oxidation in metamorphism. In: Abelson PH (ed) Researches in geochemistry. John Wiley and Sons, New York, pp 397–426

Eugster HP, Wones DR (1962) Stability relations of the ferruginous biotite, annite, J Petrol 3:82–125

Ferrow E, Annersten H (1984) Ferric iron in trioctahedral micas. Univ Uppsala UUDMP Res Rep 39

Ferry JM, Spear F (1978) Experimental calibration of the partitioning of Fe and Mg between biotite and garnet. Contrib Mineral Petrol 66:113–117

Fonarev VI, Konilov AN (1986) Experimental study of Fe-Mg distribution between biotite and orthopyroxene. Contrib Mineral Petrol 93:227–235

Frantz JD, Marshall WL (1984) Electrical conductances and ionization constants of salts, acids, and bases in supercritical aqueous fluids. I. Hydrochloric acid from 100 to 700° C and at pressures to 4000 bars. Am J Sci 284:651–667

Grevel KD, Chatterjee ND (1992) A modified Redlich-Kwong equation of state for H_2-H_2O fluid mixtures at high pressures and at temperatures above 400° C. Eur J Mineral 4:1303–1310

Hamilton DL, Henderson CMB (1968) The preparation of silicate compositions by a gelling method. Miner Mag 36: 832–838

Hazen RM, Wones DR (1972) The effect of cation substitutions on the physical properties of trioctahedral micas. Am Mineral 57:103–129

Hewitt DA, Wones DR (1975) Physical properties of some synthetic Fe-Mg-Al trioctahedral biotites. Am Mineral 60:854–862

Hewitt DA, Wones DR (1981) The annite-sanidine-magnetite equilibrium (abstract) GAC-MAC J Annu Meet Calgary Abstr 6:A-66

Hewitt DA, Wones DR (1984) Experimental phase relations of the micas. In: Bailey SW (ed) Micas. (Reviews in mineralogy, vol 13) Book Crafters, Chelsea, Michigan, pp 201–256

Holland TJ, Powell R (1985) An internally consistent thermodynamic dataset with uncertainties and correlations. 2. Data and results. J metamorphic Geol 3:343–370

Holland TJB, Powell R (1990) An enlarged and updated internally consistent thermodynamic dataset with uncertainties and correlations: the system K_2O-Na_2O-CaO-MgO-MnO-FeO-Fe_2O_3-Al_2O_3-TiO_2-SiO_2-C-H_2-O_2. J metamorphic Geol 8:89–124

Kohn MJ, Spear FS (1991) Error propagation for barometers. 2. Application to rocks. Am Mineral 76:138–147

McMullin DWA, Berman G, Greenwood HJ (1991) Calibration of the SGAM thermobarometer for pelitic rocks using data from phase-equilibrium experiments and natural assemblages. Can Mineral 29:889–908

Moecher DP, Chou IM (1990) Experimental investigation of andradite and hedenbergite equilibria employing the hydrogen-sensor technique, with revised estimates of $\Delta_f G^0_{m,298}$ for andradite and hedenbergite. Am Mineral 75:1327–1341

O'Neill HStC (1987a) Free energies of formation of NiO, CoO, Ni_2SiO_4, and Co_2SiO_4. Am Mineral 72:280–291

O'Neill HStC (1987b) Quartz-fayalite-iron and quartz-fayalite-magnetite equilibria and the free energy of formation of fayalite (Fe_2SiO_4) and magnetite (Fe_3O_4). An Mineral 72: 67–75

O'Neill HStC (1988) Systems Fe-O and Cu-O: thermodynamic data for the equilibria Fe-"FeO", Fe-Fe_3O_4, "FeO"-Fe_3O_4, Fe_3O_4-Fe_2O_3, Cu-Cu_2O, and Cu_2O-CuO from emf measurements. Am Mineral 73:470–486

Partin E, Hewitt DA, Wones DR (1983) Quantification of ferric iron in biotite (abstract). Geol Soc Am Abstr Program 15:659

Powell R (1985) Geothermometry and geobarometry: a discussion. J Geol Soc London 142:29–38

Powell R, Holland TJB (1985) An internally consistent thermodynamic dataset with uncertainties and correlations. 1. Methods and a worked example. J metamorphic Geol 3:327–342

Redhammer GJ, Beran A, Dachs E, Amthauer G (1993) A Mössbauer and X-ray diffraction study of annites synthesized at different oxygen fugacities and crystal chemical implications. Phys Chem Miner 20:382–394

Robie RA, Hemingway BS, Fisher JR (1978) Thermodynamic properties of minerals and related substances at 298.15 K and 1 bar (10^5 pascals) pressure and at higher temperatures. US Geol Surv Bull 1452

Rutherford MJ (1969) An experimental determination of iron biotite-alkali feldspar equilibria. J Petrol 10:381–408

Wolfram Research Inc (1993) Mathematica, version 2.1. Wolfram Research Inc

Wones DR, Burns R, Carroll B (1971) Stability and properties of annite. Trans Am Geophys Union 52:369–370